J Mater Sci (2010) 45:1211–1219
DOI 10.1007/s10853-009-4067-6

Microstructural effects on the phase transitions and the thermal evolution of elastic and piezoelectric properties in highly dense, submicron-structured $NaNbO_3$ ceramics

A. Moure · T. Hungría · A. Castro · L. Pardo

Received: 17 July 2009 / Accepted: 22 November 2009 / Published online: 10 December 2009

Abstract The dielectric, piezoelectric and elastic coefficients, as well as the electromechanical coupling factors, of $NaNbO_3$ submicron-structured ceramics have been obtained by an automatic iterative method from impedance measurements at resonance. Poled thin discs were measured from room temperature up to the depoling one, close to 300 °C. Dielectric thermal behaviour was determined also for unpoled ceramics up to the highest phase transition temperature. Ceramics were processed by hot-pressing from mechanically activated precursors. Microstructural effects on the properties are discussed. The suppression of the classical maximum in dielectric permittivity in unpoled ceramics at the phase transition at 370 °C was found when a bimodal distribution of grain sizes, with a population of average grain size of 110 nm in between much coarser grains, is observed. The appearance of a phase transition at 150 °C took place when Na vacancies are minimised. The occurrence of a non-centrosymmetric, ferroelectric phase, in the unpoled ceramic from room temperature to ~300 °C, highly polarisable resulting in high ferro–piezoelectric properties was also observed in the ceramic which presents grain size below 160 nm. Maximum values of $k_p = 14\%$, $d_{31} = -8.7 \times 10^{-12}$ C N^{-1} and $N_p = 3772$ Hz m at room temperature, and $k_p = 18\%$, $d_{31} = -25.4 \times 10^{-12}$ C N^{-1} and $N_p = 3722$ Hz m at 295 °C were achieved in the best processing conditions of the ceramics.

A. Moure (✉)
Instituto de Cerámica y Vidrio, CSIC, C/Kelsen, 5,
28049 Madrid, Spain
e-mail: alberto.moure@icv.csic.es

T. Hungría · A. Castro · L. Pardo
Instituto de Ciencia de Materiales de Madrid, CSIC,
Cantoblanco, 28049 Madrid, Spain

Introduction

Alkaline niobates are considered good candidates to be an alternative for the substitution of commercial piezoceramics [1, 2], which use highly toxic lead oxide in their processing. The solid solution with $K_{0.5}Na_{0.5}NbO_3$ composition is known to have piezoelectric properties at room temperature ($d_{33} \sim 80 \times 10^{-12}$ C N^{-1}) [3] that allows nowadays its commercial applications. Recently, it has been reported that d_{33} can be increased to 148×10^{-12} C N^{-1} in ceramics processed by spark plasma sintering [4]. The highest piezoelectric values by now for niobates-based ceramics have been reported for textured $(K_{0.44}Na_{0.52}Li_{0.04})$ $(Nb_{0.84}Ta_{0.10}Sb_{0.06})O_3$ compositions ($d_{33} = 416 \times 10^{-12}$ C N^{-1}) [5]. This result shows the potential of this family of compounds as lead-free piezoelectrics.

Amongst alkaline niobates, sodium niobate, $NaNbO_3$, is of particular interest because a number of solid solutions with good ferroelectric and piezoelectric properties [6–8] are based on this compound. It is antiferroelectric at room temperature [9], but the application of an electric field or the substitution of Na by Li [10] or K [11] induces a ferroelectric phase that provides piezoelectric activity, of interest mainly in high frequency devices. It presents a large number of polymorphic phases, variants of lower symmetry from the ideal perovskite structure. It undergoes six phase transitions [12] from the non-polar high temperature phases (cubic *Pm*3*m*, tetragonal *P*4/*mbm* and Orthorhombic *Ccmm* and *Pnmm*) to the antiferroelectric room temperature phase (Orthorhombic *Pbcm*) and the low temperature ferroelectric one (Rhombohedral *R*3*c*).

As for every polar oxide ceramic, the functional properties, such as piezoelectricity, of the alkaline niobate ceramics depend on the grain size, a phenomenon

commonly referred to as 'size effect.' Its importance has increased during the recent years within the nanotechnology field. Some of these effects are well known in ferroelectric ceramics with perovskite-like structure, as the increase of the dielectric permittivity in $BaTiO_3$ down to a critical grain size [13, 14]. However, there are still a lot of open questions about the size effect's influence on the ferroelectric ceramics properties.

In the particular case of the $NaNbO_3$, it has been recently observed that the grain size reduction to submicron values produces a series of phase transformations due to the increasing internal pressures [15]. The appearance of a non-centrosymmetric structure in particle sizes below 400 nm improves the piezoelectric activity, as PFM studies of displacement against voltage show [16]. These phenomena can clearly influence the behaviour with temperature of nano- and submicron-structured $NaNbO_3$ ceramics [17], where several phase transitions occur. In this sense, some studies [18–20] were focused on the analysis of the transitions in the polar phase of ceramics with $Na_{1-x}Li_xNbO_3$ compositions, involving dielectric, thermal expansion and pyroelectric current measurements. Although the phase transitions affect the thermal stability of their piezoelectric properties, not many studies [21, 22] are there in the literature regarding the evolution of the piezoelectric properties (electromechanical coupling factors or piezoelectric coefficients d_{ij}) with temperature.

It is known that the processing by classical methods of ceramics with alkaline niobate compositions in general, and $NaNbO_3$ in particular, shows difficulties in obtaining densities close to the theoretical values [10, 23]. This classical method involves high temperatures and long reaction times, produces the volatilisation of the alkali metal, leads to poor compositional homogeneity and provides products with large particles, and finally, ceramics with the undesirable phenomena of exaggerated grain growth. The authors have recently carried out [24] a quantitative analysis of $NaNbO_3$ ceramics microstructures obtained from mechanical activation of different precursors. It was shown that highly dense ceramics (down to 0.4% of porosity) can be obtained at relatively low hot-pressing temperatures (1000 °C). This allows obtaining submicron-structured ceramics with single grain size distributions with average grain sizes ranging from 110 to 390 nm.

In this study, the thermal behaviour of the piezoelectric, elastic and dielectric properties of $NaNbO_3$ ceramics has been determined with the aim of analysing the microstructural effects on the functional properties of $NaNbO_3$ ceramics in the temperature range of piezoelectric activity. The ceramics used for this study were obtained by mechanical activation of several reagents and different hot-pressing conditions. It provides microstructures with different porosity and submicron grain size.

Experimental procedure

Ceramics with $NaNbO_3$ (NN) composition have been prepared from precursors obtained by mechanical activation through three different routes. The details of the precursor processing and its characterisation can be found elsewhere [25]. Ceramic discs of diameter (d) to thickness (t) ratio 1:10 were obtained by hot pressing at 200 MPa, 1000 °C-2 h (hereinafter called ceramics C-NN, DOH-NN-1 and O-NN-1, from Na_2CO_3, NaOH and Na_2O precursors, respectively) and 1100 °C-2 h (hereinafter called ceramics DOH-NN-2 and O-NN-2) in a single thermal treatment from the mechanically activated precursors. The microstructural study of the ceramics has been previously carried out [24]. Hot pressing allowed highly dense (down to 0.4% for DOH-NN-1 ceramics) and mechanically stable submicron-structured ceramics to be obtained. The grain size was characterised as the equivalent diameter to a circular shape ($D_{eq} = 2(A/\pi)^{1/2}$), calculated from the measured grain area (A), which is a good approach since grains are equiaxed [24, 26]. Average grain sizes (D_{equiv}) range from 110 to 390 nm. Intermediate sintering stages were observed for the O-NN-1 and DOH-NN-1 ceramics, and bimodal lognormal grain size distributions were measured. Homogeneous microstructures with single lognormal distributions were obtained for the rest of the ceramics. All the microstructural parameters that are of interest for this study and drawn from the previous study [24] are summarised in Table 1.

For the dielectric characterisation before poling, ceramics with 0.7–1.0 mm in thickness with Pt-painted electrodes sintered at 900 °C were prepared. Impedance measurements at 1 kHz and as a function of temperature were carried out with a HP4194A analyser, in an experimental set-up for the temperature control described in [27]. The heating and cooling rates were 2 °C/min. From these experimental data and a geometry factor thickness/area, complex dielectric permittivity, $\varepsilon^* = \varepsilon' - i\varepsilon''$, and dielectric losses, $\tan\delta = \varepsilon''/\varepsilon'$, were obtained.

After the dielectric measurements, the ceramics were poled up to saturation in a silicon oil bath at 120–180 °C with electric fields as high as 6000 kV/m. The dielectric (ε_{33}^{T} at the resonance frequency), elastic (s_{11}^{E} and s_{12}^{E}) and piezoelectric coefficients (d_{31}), including all losses, as well as the electromechanical coupling factors (k_p), and the frequency numbers (N_p) corresponding to the radial resonance mode of thin disc-shaped ceramics at room temperature were measured by the automatic iterative method according to Alemany et al., described elsewhere [28]. Measurements were also carried out as a function of temperature with a procedure also explained elsewhere [29] using a HP4192A impedance analyser.

Table 1 Piezoelectric, elastic and dielectric characterisation at room temperature of the planar resonance of thin discs of $NaNbO_3$ hot-pressed ceramics

$NaNbO_3$ ceramics	C-NN 1000 °C	O-NN-2 1100 °C	DOH-NN-1 1000 °C	DOH-NN-2 1100 °C
Porosity (%)	6.4 ± 0.8	3.8 ± 0.3	0.40 ± 0.02	2.10 ± 0.06
$\langle D_{eq} \rangle$ (nm)	220	240	160*	390
σ_{Deq} (nm)	120	120	80	230
$T_C^{heating}$ (°C)	355	371	307	371
d_{33} (10^{-12} C N^{-1})	40	24	38	32
k_p (%)	14	8	12	12
d_{31} (10^{-12} C N^{-1})	−8.7 + 0.09i	−5.2 + 0.12i	−7.8 + 0.06i	−7.2 + 0.03i
N_p (Hz m)	3571	3535	3252	3778
s_{11}^E (10^{-12} m^2 N^{-1})	8.5 − 0.04i	7.8 − 0.01i	9.7 − 0.03i	6.7 − 0.008i
Q_m (s_{11}^E)	200	660	344	863
s_{12}^E (10^{-12} m^2 N^{-1})	−1.4 + 0.0065i	−1.9 + 0.0031i	−2.2 + 0.0211i	−1.6 + 0.0018i
Q_m (s_{12}^E)	217	606	106	859
ε_{33}^T	144 + 1.77i	154 + 1.44i	133 + 1.64i	158 + 1.79i

Microstructural factors (percentage of porosity and mean value ($\langle D_{eq} \rangle$) and standard deviation (σ_{Deq}) of the grain size distributions) reported in Ref. [24] are also shown (measurement error for grain size: ±20 nm; * bimodal grain size distribution, value shown corresponds to the largest grain size)

Results

Figures 1 and 2 show the evolution with temperature of the dielectric permittivity, ε', and the loss factor, tan δ, at 1 kHz for unpoled NN ceramics. A sharp dielectric anomaly on heating with strong thermal hysteresis (∼50 °C) is observed at ∼370 °C for DOH-NN-2, and at 355 °C for C-NN ceramics. This is currently ascribed in the literature to the first-order phase transition from the antiferroelectric RT phase [12, 18]. A maximum of ε' at the phase transition (T_C on heating) is not well defined for the O-NN-1 ceramics. The O-NN-2 ceramic phase transition can be observed but with a strong diffuse character in contrast with the first-order phase transition shown by the rest of the ceramics. There is a displacement of T_C on heating with respect to the reported one for $NaNbO_3$ single crystals and coarse-grained ceramics (T_C ∼ 370 °C) [12, 18], severe for the DOH-NN-1 (T_C ∼ 306 °C) and moderate for the C-NN ceramics (T_C ∼ 355 °C). The inset in Fig. 1a represents the details of the temperature dependence of the dielectric permittivity up to 250 °C. An anomaly at ∼150 °C is observed for the C-NN ceramics. The O-NN-1 ceramics have the largest values of dielectric losses. For the O-NN-1 ceramics, a tail close to room temperature is observed. It is probably related with conduction phenomena, and is beyond the scope of this study.

Figure 3 shows the peaks of the real part of the complex impedance (R = a.c. resistance) and the real part of the complex admittance (G = a.c. conductance) at the planar resonance modes of the poled ceramic discs and their reproduction from the calculated parameters by the iterative

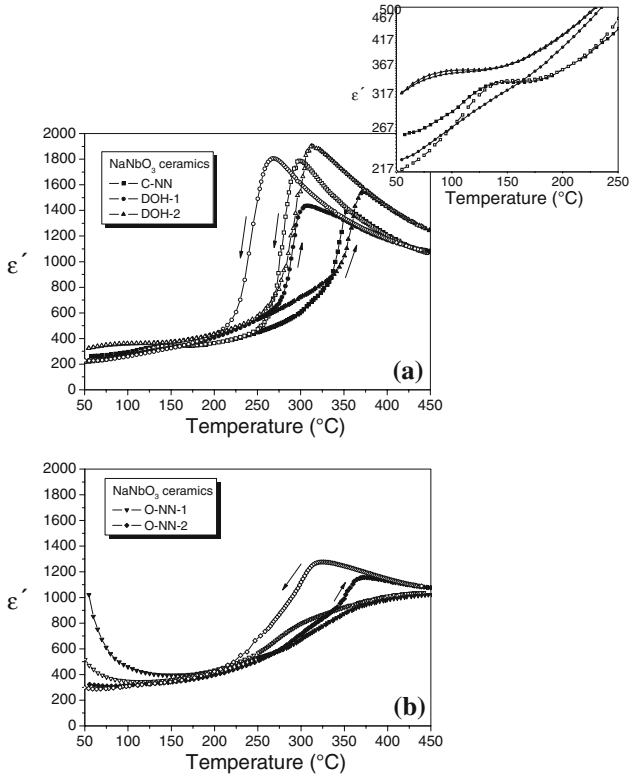

Fig. 1 Real part of the dielectric permittivity at 1 kHz as a function of temperature for $NaNbO_3$ hot-pressed ceramics (*solid symbols*: heating; *open symbols*: cooling). *Inset*: Magnifications of figure from 50 to 250 °C

method at resonance for all the $NaNbO_3$ hot-pressed ceramics, except for the O-NN-1 ones. The spectra are represented at room temperature (RT) and at 310 °C only

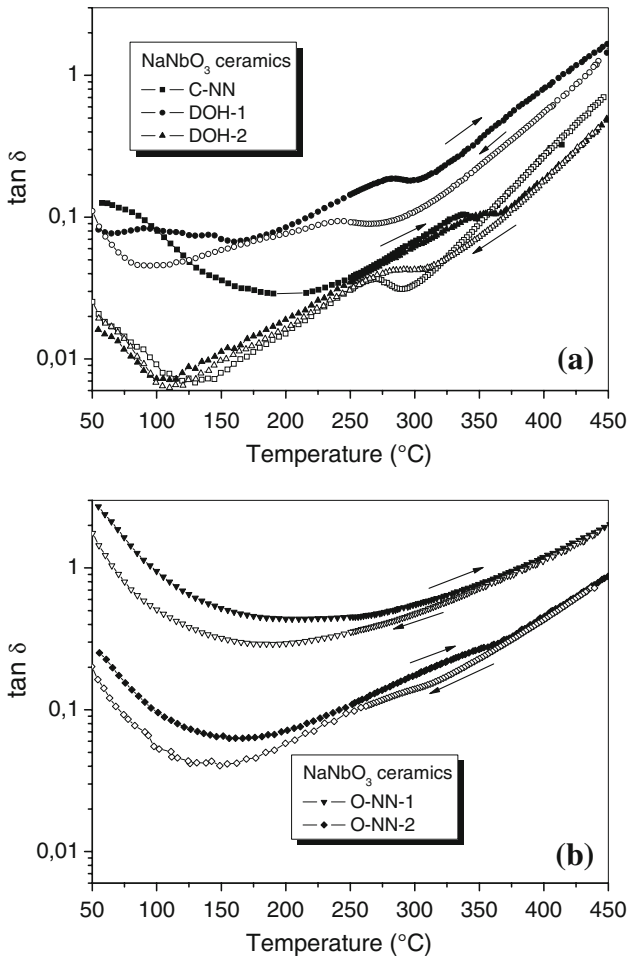

Fig. 2 Dielectric losses at 1 kHz as a function of temperature for $NaNbO_3$ hot-pressed ceramics (*solid symbols*: heating; *open symbols*: cooling)

for the ceramics for which the resonances are clearly distinguished (C-NN and DOH-NN-2) at that temperature.

Dielectric, elastic and piezoelectric coefficients, as well as the electromechanical coupling factors and frequency numbers, calculated from the resonance spectra at room temperature (Fig. 3) are shown in Table 1. The peaks are wider for the C-NN ceramics, as it corresponds to lower values of the mechanical quality factors, Q_m (s^E_{11}) and Q_m (s^E_{12}), shown in Table 1. The highest piezoelectric activity (highest k_p and d_{31} values) corresponds to the C-NN ceramic, while the elastic parameters, (N_p, s^E_{11}, s^E_{12}), show that DOH-NN-2 is the stiffest ceramic and DOH-NN-1 the most compliant.

Figure 4a shows the evolution with temperature of the real part of the planar electromechanical coupling factor (k_p) of $NaNbO_3$ ceramics. Except for O-NN-2, which has a softer decrease over a wider temperature range, all of them present the same shape, with a variation from room temperature up to ~300 °C and a sharp decrease from that temperature. At ~300 °C, k_p abruptly decreases, but there is still a measurable electromechanical resonance for C-NN and DOH-NN-2. At ~325 °C none of the ceramics presents piezoelectric activity. This is also a lower temperature than the one of the phase transition from the antiferroelectric phase measured on heating for the unpoled ceramics (Fig. 1). The highest values in all the temperature ranges under study correspond to the C-NN ceramic, while the O-NN-2 one presents the lowest ones. The curve for the O-NN-1 ceramic has not been measured. The reason is that this ceramic presents a high conductivity and is very difficult to pole. Ultrafine intergranular porosity accompanying the family of smaller grain sizes of its bimodal grain size distribution was observed in this ceramic. Porosity is detrimental for the grain connectivity needed for the establishing of a homogeneous electric field in the ceramic. The achieved piezoelectric activity is very low, ($d_{33} = 6 \times 10^{-12}$ C N^{-1}), and the ceramic is rejected for further measurements as a function of the temperature as it is of no practical interest.

Figure 4b shows the evolution with temperature of the real part of the piezoelectric coefficient d_{31}. It has the same dependence on processing conditions and measuring temperatures as k_p, but the increase from room temperature up to ~300 °C is remarkable for C-NN and DOH-NN-1 ceramics and is almost three times the value at 50 °C. The highest values also correspond to the C-NN ceramic. It has its maximum at 295 °C, where $d_{31} = -25.4 \times 10^{-12}$ C N^{-1}.

Figure 5a shows the dependence on temperature of the planar frequency number N_p. In all the curves, there is a decrease in N_p, meaning a softening of the ceramic, up to the temperatures where piezoelectric activity tends to zero (Fig. 4a, b). Then, N_p rapidly increases. This increase occurs also over a wider temperature interval (from ~250 °C) for the O-NN-2 ceramic than for the rest. The DOH-NN-2 ceramic has the highest values in all the temperature range, while the DOH-NN-1 one has the lowest values.

The measurement of the resonance frequency, and thus of $N_p = f_s^p d$ is much more accurate than the calculation of any of the obtained parameters from the resonance spectrum. Despite this, the evolution with temperature of the elastic compliances, s^E_{11} and s^E_{12}, shown in Fig. 5b, c, shows also the main facts described for the thermal evolution of N_p. The highest values correspond to the DOH-NN-1 ceramic, and the lowest values to the DOH-NN-2 one. A jump in the s^E_{11} and s^E_{12} coefficients at 150 °C is observed only for the C-NN ceramic.

Discussion

The processing of the ceramics from three different types of powders and two hot-pressing temperatures gave place

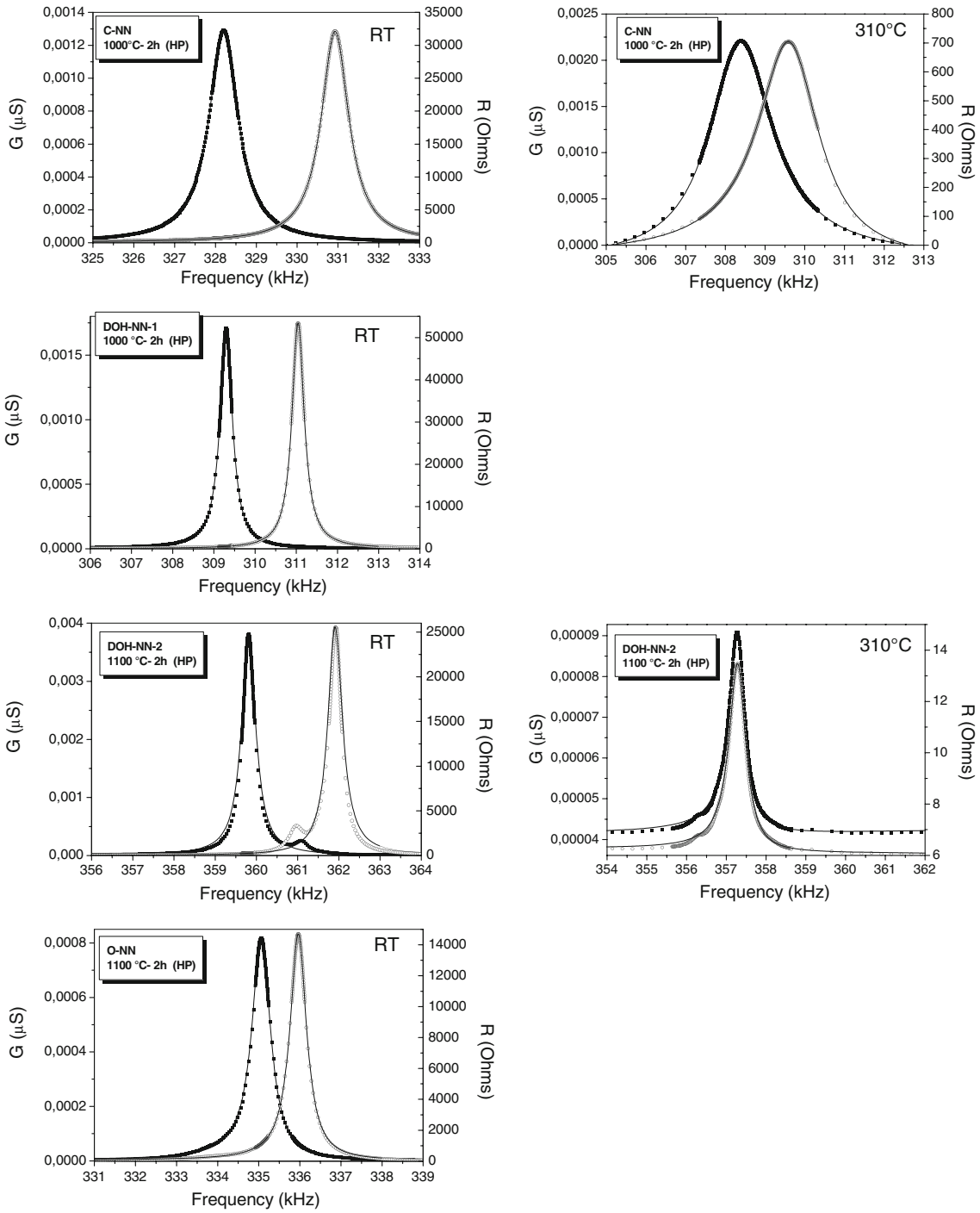

Fig. 3 *R* and *G* curves at room temperature (RT) and at 310 °C of resonance (*closed squares*) and anti-resonance (*open circles*) and reproduction from the constants obtained by the iterative method (*line*) at planar resonance of $NaNbO_3$ hot-pressed ceramics

to variations of the microstructural factors that define the ferro–piezoelectric performances found in each ceramic. A certain number of the observed characteristics cannot be easily understood as classical grain size and porosity dependence. The explanation of all these characteristics needs analysis of other ceramic microstructural features.

This is the case of the lack of a well-defined maximum in T_C on heating or cooling, together with the lowest values in the curve of the unpoled dielectric permittivity, for O-NN-1 ceramics. These are accompanied by the small piezoelectric activity of the O-NN-1 ceramic ($d_{33} = 6 \times 10^{-12}$ C N^{-1}). In order to understand this, we have to take

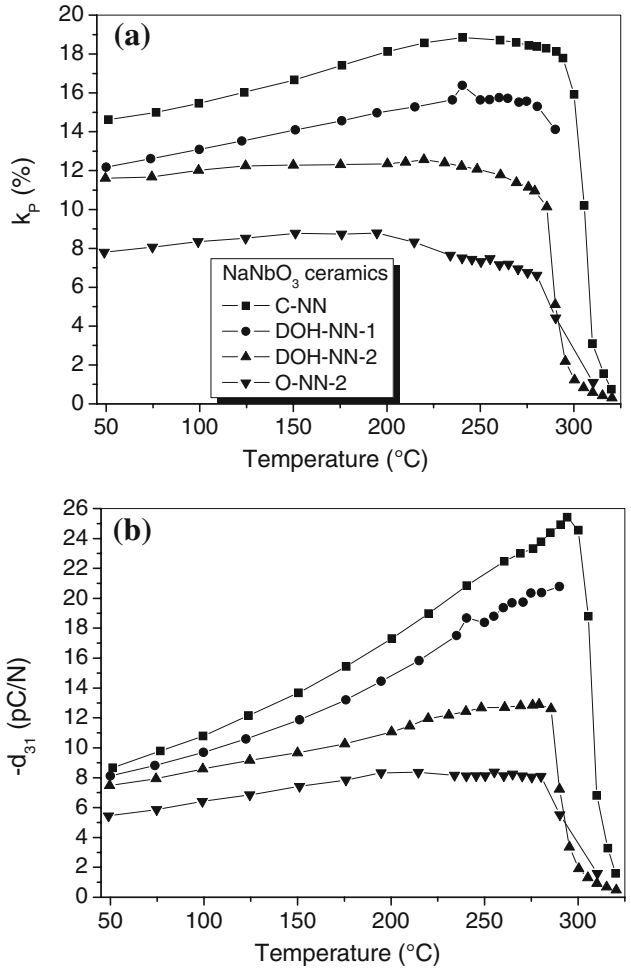

Fig. 4 Thermal evolution of **a** Planar electromechanical factor k_p and **b** real part of the piezoelectric coefficient d_{31} for $NaNbO_3$ hot-pressed ceramics

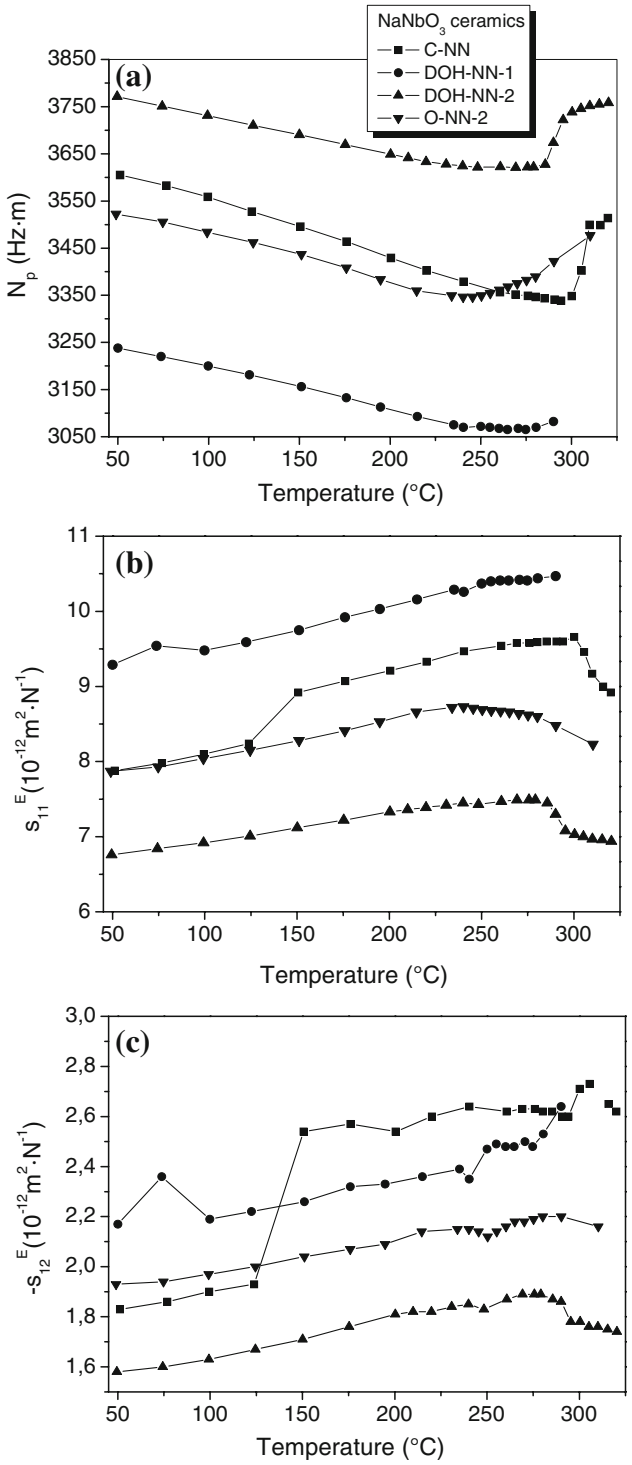

Fig. 5 Thermal evolution of **a** planar frequency number N_p; **b** compliance coefficient s_{11}^E and **c** compliance coefficient s_{12}^E for $NaNbO_3$ hot-pressed ceramics

into consideration the recently and newly published information on $NaNbO_3$ powder nanoparticles structure. Raman spectroscopy studies on $NaNbO_3$ powder samples have shown a diffuse phase transition [30] at 180 °C, with no other changes taking place at higher temperatures, in particles with sizes <70 nm. On increasing grain size to the submicron range (200–400 nm), a noncentrosymmetric structure at room temperature is developed with a phase transition taking place in a temperature interval from 310 to 330 °C [15]. For particle sizes >1 μm, the phase transition is observed at 370 °C, corresponding to the commonly measured phase transition for single crystals and unpoled ceramics with grain size in the micron range [18]. The reduced ceramic grain size of the O-NN-1 sample seems to inhibit the polarisability of the lower size population, suppressing the antiferroelectric phase before poling and the phase transition from it, as observed by the lack of anomalies above 180 °C in the Raman spectra of particles below 70 nm. The microstructure of the O-NN-1 can be described as antiferroelectric-isolated regions with high dielectric permittivity surrounded by a nano-grainsize-generated non-polar phase regions, and thus with low dielectric permittivity, that present an overall low dielectric

permittivity and polarisability, due to lack of continuity between electrodes of the former. This effect is the well-known one for the piezoelectric composites consisting of isolated ferroelectric particles of high permittivity dispersed in a low permittivity polymer (0–3 connectivity composites) [31].

The strong T_C reduction on heating for unpoled DOH-NN-1 ceramic is accompanied by one of the best piezoelectric properties. It is remarkable that the shift to lower temperatures of T_C on heating in the transition from the phase at room temperature for the unpoled ceramics (up to 64 °C reduction for DOH-NN-1 with respect to DOH-NN-2) revealed by the dielectric permittivity versus temperature measurements (Fig. 1) does not have influence on the temperature range of ferro–piezoelectric activity of the ceramics after poling (Figs. 4 and 5). All the ceramics, including the DOH-NN-1 one, keep ferro–piezoelectric activity up to ~295 °C. This depoling temperature and the shape of the curve are similar to those reported in [21, 22] for $NaNbO_3$ and Li-doped $NaNbO_3$ with low Li contents. It is directly related with the temperature evolution of the remnant ferroelectric polarisation in $NaNbO_3$-poled ceramics [32]. Therefore, the transition from the ferroelectric phase that was induced by poling to a non-piezoelectric, centrosymmetric one, seems to take place near 300 °C for all the ceramics.

The DOH-NN-1 ceramic presents a bimodal grain size distribution in the limit between submicron- and nano-structure. One of the populations of this bimodal distribution is built-up by well-formed grains with an average grain size of 160 nm. The second population consists of clusters, with an internal structure of grains in coalescence with an average grain size well below 100 nm [24] (Fig. 6a). Such microstructure seems to be in the origin of the distinct permittivity versus temperature curve with a T_C on heating at ~300 °C. Figure 6a, b depict the dielectric permittivity values before (ε' at 3×10^5 Hz) and after poling (low-frequency dielectric constant ε_{33} measured at 300 kHz, which is the resonance frequency for poled sample [28]) of the DOH-NN-1 and 2 ceramics, respectively. For the DOH-NN-2, there is a strong difference between the shapes of the two curves, as it corresponds to the fact that they are measurements of two distinct phase transitions taking place at different temperatures. While the curve for the unpoled sample measures a phase transition from the antiferroelectric phase, the curve for the poled one measures a phase transition from the ferroelectric induced by poling. On the contrary, the shape of the curves for DOH-NN-1 is identical, suggesting that both measurements correspond to the same phase transition. That is to say, the same phase transition takes place for both the unpoled and poled samples. Poled samples present the transition from a field-induced ferroelectric phase. This means that in the unpoled state of the DOH-NN-1 ceramic the very fine and dense microstructure stabilises a ferroelectric phase, in the absence of the electric

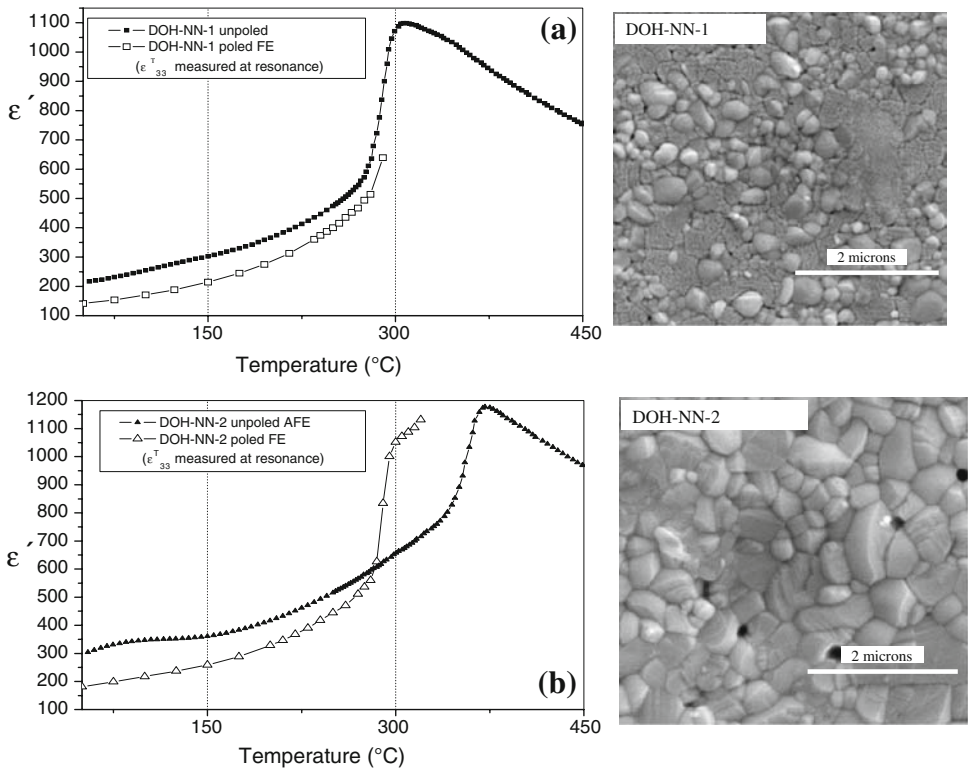

Fig. 6 Real part of the dielectric permittivity as a function of temperature for poled and unpoled **a** DOH-NN-1 ceramics and **b** DOH-NN-2 ceramics (*solid symbols*: unpoled ceramics, measured at 3.6×10^5 Hz; *open symbols*: poled ceramics, measured at resonance frequencies). *Inset*: SEM micrographs of polished and thermally etched surfaces of the corresponding ceramics

field and below the transition temperature (300 °C), instead of the antiferroelectric one. The parallel behaviour of the thermal evolution for unpoled and poled DOH-NN-1 ceramics shows that the unpoled ceramic has, similar to what was found by Raman study for submicron particles from room temperature to ~300 °C [15], a highly polarisable non-centrosymmetric phase, stabilised by the very fine and dense microstructure.

Such phenomenon is not unique. On the contrary, in artificially layered ferroelectric–dielectric superlattices, the electrostatic coupling between alternating thin ferroelectric and dielectric layers is able to induce a polarisation in the latter, and when the dielectric is sufficiently polarisable, this yields an uniformly and highly polarisable phase and the appearance of high dielectric permittivity values and tuning of the phase transition temperature [33]. Similar electrostatic coupling could take place in between nanoregions of antiferroelectric, polarisable phase, and those of ferroelectric one. Such nanoregions, as observed in $NaNbO_3$ single crystals, would be due to local differences in Na vacancies content [34]. The coupling would be favoured by the high density and very fine grain of the DOH-NN-1 ceramics.

The high temperature phase after the transition at ~300 °C for the DOH-NN-1 ceramic must be different relative to the rest of the ceramics. For these, the antiferroelectric (polar and non-piezoelectric) room temperature phase must take place after depolarisation and up to the transition at 370 °C (Fig. 1). The absence for DOH-NN-1 unpoled ceramics of other dielectric anomalies above the depolarisation temperature (Fig. 1) suggests that the transition at 306 °C takes place to another phase. This will also explain the different a.c. conductivity at resonance and subsequent difficulties in the material parameters' calculation after the phase transition in the DOH-NN-1 ceramics.

The anomaly in the dielectric permittivity at ~150 °C in both heating and cooling runs, clearly observed in the insets of Fig. 1 only for the C-NN ceramics, shows a second-order phase transition previously reported in $NaNbO_3$ single crystals [35]. It has also been observed in Raman spectroscopy studies for $NaNbO_3$ powder [36], in both heating and cooling runs, and for spark plasma-sintered ceramics [32]. The anomaly is also observed here as a jump in the elastic compliance coefficients, s_{11}^E and s_{12}^E (Fig. 5b, c, respectively). In this case, the measurement is performed after poling, when a ferroelectric phase is induced by the application of an electric field [32]. It can be concluded that the phase transition at ~150 °C is produced inside ferroelectric regions induced, which most likely exist also in unpoled ceramics. The existence at room temperature of a ferroelectric phase (called as M) has been reported in unpoled single crystals of $NaNbO_3$ with a structure different from the ferroelectric phase (called Q) resulting from the application of an electric field. The observed phase transition occurs between the M and the Q phase. In the same study [34], it is also proposed that in regions where Na composition is lower than the stoichiometric one, and many Na vacancies exist, the occurrence of an antiferroelectric structure (P) is favoured. When DOH-NN or O-NN precursors are used, Na-sites' defects can increase, by evaporation. It would favour the P antiferroelectric phase [34] and inhibits the formation of M phases. This explains why, in those cases, the phase transition at ~150 °C is not observed. It is also possible that the long milling time for the precursors of the C-NN ceramics (30 days [25]) could result in a better mixing of the powder as well as the incipient mechanosynthesis, which reduces the stoichiometric faults. The existence of these regions of ferroelectric phase in the unpoled state is responsible for the C-NN ceramics piezoelectric coefficients to be the highest ones amongst all the ceramics obtained in this study (Table 1).

The shape of the temperature dependence of the elastic properties (N_p, s_{11}^E, s_{12}^E) is in good agreement with the increase in Young's modulus reported in sodium niobate ceramics with 1% Li content [19]. The differences among the ceramics (Fig. 5) seem to indicate a double influence of the microstructure due to porosity and the homogeneity of the ceramics grain size. The C-NN and O-NN-2 ceramics have a similar grain size (220 and 240 nm, respectively), but N_p (Fig. 5a) is higher for the latter due to their lower porosity (3.8 compared with 6.4% of porosity, see Table 1). Besides, a comparatively higher vacancies content in O-NN-2 (higher processing temperature favours Na evaporation) produces an electromechanical stiffening due to domain wall trapping by vacancies [29], which also reduces the extrinsic component of the domain walls to the piezoelectric activity, reducing the d_{31} coefficient and coupling factor (Fig. 4). The trend with porosity content is the opposite if the DOH-NN-1 (0.4%) and DOH-NN-2 (2.1%) ceramics are compared. As Fig. 6 shows, the former ceramic has a bimodal grain size distribution that contains clusters, with an internal structure of grains in coalescence. The increase of the hot-pressing temperature to 1100 °C gives place to a single grain size distribution in DOH-NN-2. The clusters in DOH-NN-1 must be softer, and together with the relatively lower content of vacancies of these ceramics, make them the most compliant.

Conclusions

Microstructural effects on the dielectric, piezoelectric and elastic properties of dense submicron-structured $NaNbO_3$

ceramics were studied up to the same temperatures as, or to those higher than, the depoling ones.

For dense ceramics with similar submicron average grain size and that show single grain size distributions, the unpoled dielectric permittivity as a function of temperature presents the usual facts measured for NN single crystals and coarse-grain ceramics. The differences of the coefficients obtained from to the electromechanical resonance, the phase transition at 150 °C for C-NN, the strong dielectric permittivity decrease and dielectric losses increase for O-NN-2, can be interpreted in terms of the differences in the composition (secondary phases).

For dense ceramics with a bimodal grain size distribution that contains a great extent of a submicron grains population, with ultrafine intergranular porosity in between grains of microns size, an inhibition of the antiferroelectric phase in the finer grain population is observed, suppressing the maximum of the dielectric permittivity with temperature. The non-polar phase surrounding the antiferroelectric grains causes a reduction of the dielectric permittivity and polarisability, 0–3 connectivity-type composite effect, in the O-NN-1 ceramic that greatly reduces the ferro–piezoelectric activity after poling.

The second of the grain size effects, not yet reported in the literature for ceramics, was found in the ceramic with the highest density having also a bimodal grain size distribution. The unpoled ceramic has a microstructure-stabilised non-centrosymmetric ferroelectric phase. It is a highly polarisable phase which contributes to the enhancement of the dielectric and piezoelectric properties.

In summary, these results show the microstructural factors that affect the phase transitions and piezoelectric performance of highly dense, submicron-structured $NaNbO_3$ ceramics and improve the coupling factors (up to $k_p \sim$ 12–14%) and mechanical quality factors (up to Q_m (s_{11}^E) > 800). This knowledge has practical interest in the achievement of high performance lead-free piezoelectric solid solution systems containing $NaNbO_3$.

Acknowledgements Authors thanks the EC project "LEAF" G5RD-CT2001-00431, EC project "PIRAMID" G5RD-CT-2001-00456 and MAT2001-4818E (MCyT Spain), MAT2001-0561, CAM (07N/0076/2002), MAT2004-00868 and MAT2007-61884 projects, COST 528 and COST 539 Actions, Thematic Network CE (contract G5RT-CT2001-05024) and Network of Excellence, 6FP-CE (NMP3-CT-2005-515757). Drs. A. Moure and T. Hungría are indebted to the CSIC (MICINN) of Spain for the "Junta de Ampliación de Estudios" contracts (Refs JAEDOC087 and JAEDOC082, respectively). Thanks are also given to Ms. M. Antón (working under a FINNOVA2003-LEAF grant) for the powder samples preparation. Authors are indebted to late Dr. C. Alemany, for the implementation of the software used.

References

1. Cross E (2004) Nature 432:24
2. Shrout TR, Zhang SJ (2007) J Electroceram 19:111
3. Jaffe B, Cook WR, Jaffe H (1971) Piezoelectric ceramics. Academic Press, London, 1971
4. Li JF, Wang K, Zhang BP, Zhang LM (2006) J Am Ceram Soc 89:706
5. Saito Y, Takao H, Tani T, Nonoyama T, Takatori K, Homma T, Nagaya T, Nakamura M (2004) Nature 432:84
6. Raevski IP, Prosandeev SA (2002) J Phys Chem Solids 63:1939
7. Chen Z, He X, Yu Y, Hu J (2009) Jpn J Appl Phys 48:030204
8. Ma Y, Chen XM (2009) J Appl Phys 105:054107
9. Cross LE, Nicholson B (1955) J Phil Mag Ser 46:453
10. Nitta TJ (1968) J Am Ceram Soc 51:626
11. Shirane G, Newnham B, Pepinsky R (1954) Phys Rev 96:581
12. Megaw HD (1974) Ferroelectrics 7:87
13. Arlt G, Hennings D, de With G (1985) J Appl Phys 58:1619
14. Buessem WR, Cross LE, Goswami AK (1966) J Am Ceram Soc 49:33
15. Shiratori Y, Magrez A, Dornseiffer J, Haegel FH, Pithan C, Waser R (2005) J Phys Chem B 109:20122
16. Shiratori Y, Magrez A, Kasezawa K, Kato M, Röhrig S, Peter F, Pithan C, Waser R (2007) J Electroceram 19:273
17. Shanker V, Samal SL, Pradhan GK, Narayana C, Ganguli AK (2009) Solid State Sci 11:562
18. Lanfredi S, Lente MH, Eiras JA (2002) Appl Phys Lett 80:2731
19. Jiménez B, Castro A, Pardo L (2003) Appl Phys Lett 82:3940
20. Jimenez R, Hungria T, Castro A, Jimenez-Rioboo R (2008) J Phys D Appl Phys 41:065408
21. Pardo L, Durán-Martín P, Mercurio JP, Nibou L, Jiménez B (1997) J Phys Chem Solids 58:1335
22. Reznitchenko LA, Turik AV, Kuznetsova EM, Sakhnenko VP (2001) J Phys: Condens Matter 13:3875
23. Henson RM, Zeyfang RR, Kiehl KV (1977) J Am Ceram Soc 60:15
24. Moure A, Hungría T, Castro A, Pardo L (2009) J Eur Ceram Soc 29:2297
25. Hungria T, Pardo L, Moure A, Castro A (2005) J Alloys Compd 395:166
26. Ricote J, Alemany C, Pardo L (1995) J Mater Res 10:3194
27. Durán-Martín P (1997) Propiedades ferroeléctricas de materiales cerámicos con estructura tipo Aurivillius de composiciones basadas en $Bi_2SrNb_2O_9$ Tesis Doctoral UAM
28. Alemany C, Gónzalez AM, Pardo L, Jiménez B, Carmona F, Mendiola J (1995) J Phys D Appl Phys 28:945
29. Moure A, Alemany C, Pardo L (2005) J Electrochem Soc 152:F1
30. Shiratori Y, Magrez A, Fischer W, Pithan C, Waser R (2007) J Phys Chem C 111:18493
31. Lee MH, Halliyal A, Newnham RE (1989) J Am Ceram Soc 72:986
32. Wada T, Tsuji K, Saito T, Matsuo Y (2003) Jpn J Appl Phys 42:6110
33. Dawber M, Lichtensteiger C, Cantoni M, Veithen M, Ghosez P, Johnston K, Rabe KM, Triscone JM (2005) Phys Rev Lett 95:177601
34. Chen J, Feng D (1988) Phys Stat Sol (a) 109:171
35. Raevskii IP, Reznichenko LA, Smotrakov VG, Eremkin VV, Malitskaya M, Kuznetsova EM, Shilkina LA (2000) Tech Phys Lett 26:744
36. Wang XB, Shen ZX, Hu ZP, Qin L, Tang SH, Kuok MH (1996) J Mol Struct 385:1